


Research Paper

Cisplatin Prodrug-Conjugated Gold Nanocluster for Fluorescence Imaging and Targeted Therapy of the Breast Cancer

Fangyuan Zhou^{1,2*}, Bing Feng^{1*}, Haijun Yu¹, Dangge Wang¹, Tingting Wang¹, Jianping Liu¹, Qingshuo Meng¹, Siling Wang², Pengcheng Zhang¹, Zhiwen Zhang¹, Yaping Li¹

1. State Key Laboratory of Drug Research & Center of Pharmaceutics, Shanghai Institute of Materia Medica, Chinese Academy of Sciences, Shanghai 201203, China;
2. School of Pharmacy, Shenyang Pharmaceutical University, Shenyang 110016, China.

* Equal contribution to this study.

 Corresponding authors: Dr. Haijun Yu, Prof. Dr. Yaping Li; State Key Laboratory of Drug Research & Center of Pharmaceutics, Shanghai Institute of Materia Medica, Chinese Academy of Sciences, Shanghai 201203, China. E-mail: hjyu@simm.ac.cn; ypli@simm.ac.cn; Tel/Fax: +86-21-2023-1979. Or Prof. Siling Wang; School of Pharmacy, Shenyang Pharmaceutical University, Shenyang 110016, China. E-mail: wangslsy@163.com.

© Ivyspring International Publisher. Reproduction is permitted for personal, noncommercial use, provided that the article is in whole, unmodified, and properly cited. See <http://ivyspring.com/terms> for terms and conditions.

Received: 2015.11.29; Accepted: 2016.02.08; Published: 2016.03.11

Abstract

Theranostic nanomedicine has emerged as a promising modality for cancer diagnosis and treatment. In this study, we report the fabrication of fluorescence gold nanoclusters (GNC) conjugated with a cisplatin prodrug and folic acid (FA) (FA-GNC-Pt) for fluorescence imaging and targeted chemotherapy of breast cancer. The physio-chemical properties of FA-GNC-Pt nanoparticles are thoroughly characterized by fluorescence/UV-Vis spectroscopic measurement, particle size and zeta-potential examination. We find that FA-modification significantly accelerated the cellular uptake and increased the cytotoxicity of GNC-Pt nanoparticles in murine 4T1 breast cancer cells. Fluorescence imaging *in vivo* using 4T1 tumor bearing nude mouse model shows that FA-GNC-Pt nanoparticles selectively accumulate in the orthotopic 4T1 tumor and generate strong fluorescence signal due to the tumor targeting effect of FA. Moreover, we demonstrate that FA-GNC-Pt nanoparticles significantly inhibit the growth and lung metastasis of the orthotopically implanted 4T1 breast tumors. All these data imply a good potential of the GNC-based theranostic nanopatform for fluorescence tumor imaging and cancer therapy.

Key words: Theranostic Nanomedicine, Gold Nanoclusters, Fluorescence Imaging, Targeted Therapy.

Introduction

Theranostic nanoparticles (NPs) can realize simultaneous cancer diagnoses and treatment, monitor the drug delivery and evaluate the treatment efficacy by integrating multiple imaging and therapeutic functions into one single nanopatform. This might promote the clinical translation of cancer nanomedicine.(1,2) Although promising, theranostic nanomedicine is still in its infancy due to the lack of suitable nanovectors to integrate distinct functions into one single platform. So far, inorganic nanoparticles including gold nanomaterials,(3,4) quantum dots,(5) or

superparamagnetic iron oxide (SPIO) nanoparticles(6,7) had extensively been investigated for photothermal cancer therapy, fluorescence or magnetic resonance imaging (MRI) of the solid tumors. Inorganic nanoparticles coated with a polymer or protein layer had also been exploited for noncovalent drug loading and combinational cancer therapy.(8,9) However, these nanoparticles have not yet achieved wide clinical application due to the concerns about their long-term safety and surface-dependent drug-loading property.

In addition to these inorganic nanoparticles, several organic nanoparticles including paclitaxel (PTX)-loaded polymeric micelles (*e.g.*, NK105),(10) Doxorubicin/cisplatin-loaded liposomes (Doxil/Lipoplatin),(11,12) and PTX-loaded human serum albumin nanoparticles (Abraxane, (13)) have been approved or in phase III clinical trial for cancer therapy due to their superior biocompatibility, long blood circulation and high drug-loading capacity. Unfortunately, these nanoparticles tend to accumulate in the liver and spleen because of the nonspecific capture by the reticuloendothelial system (RES).(14,15) Moreover, these nanoparticles intrinsically lack diagnosis function. Additional imaging moiety is required to monitor their *in vivo* behaviour and evaluate their therapeutic outcome.(16) In past years, the emerging application of fluorescence metal (*e.g.*, gold and silver) nanoclusters has gained increased attention for fluorescence imaging,(17,18) diagnosis,(19,20) and cancer radiotherapy.(21) Gold fluorescence nanoclusters (GNC) protected with bovine serum albumin (BSA) or short peptide both display good biocompatibility, highly fluorescence emission in the near infrared (NIR) region (*i.e.*, 650-750 nm), and superior photo- and chemical stability compared to organic dyes or quantum dots.(22,23) The BSA-protected GNC has a particle size in several to ten nanometers, allows its escape from the RES absorption in the liver and quick kidney clearance, which can thus avoid liver accu-

mulation and minimize its side effect of GNCs for biomedical application.(24-26) In this study, to develop a nanoplatform for theranostic of breast cancer, we employed BSA-protected GNC nanoparticle as a dual-functional nanoplatform for drug delivery and fluorescence imaging of the tumor. The GNC nanoparticles were firstly conjugated with a reduction-sensitive cisplatin prodrug (cis,cis,trans-[Pt(NH₃)₂Cl₂(OH) (O₂CCH₂CH₂CO₂H)] (MDDP), and then functionalized with a targeting ligand folic acid (FA). FA can target the breast tumors by recognizing the folate receptor α (FR- α) overexpressed on the surface of the cancer cells. We demonstrated that using a highly aggressive 4T1 breast cancer cell line and its orthotopic tumor model, the prodrug and FA dual-conjugated GNC nanoparticles could selectively accumulate inside the tumour and the cancer cells. The nanoparticles could efficiently inhibit the growth of the primary tumor and suppress the metastasis of the cancer cells to the lung (Fig. 1).

Results and discussion

Synthesis and characterization of FA-GNC-Pt nanoparticles

BSA-protected fluorescence GNC nanoparticles were synthesized by in-situ reduction of chlorauric acid. The successful synthesis of BSA-protected GNC nanoparticles was confirmed by fluorescence spectrophotometric and imaging examination, respectively (Fig. 2a). GNC nanoparticles were firstly conjugated with hydrophilic cisplatin MDDP to obtain prodrug conjugated GNC nanoparticles (namely GNC-Pt) (see Fig. S1-3 for synthesis and characterization of the MDDP prodrug). The mass percentage of Pt in the lyophilized GNC-Pt was 0.94±0.7% as determined by using inductively coupled plasma mass spectrometric (ICP-MS) measurement. Accordingly, three MDDP molecules were conjugated on each GNC nanoparticles in average. Cisplatin was used in this study because it is a first-line anti-cancer drug used for treating a wide diversity of malignant tumors. MDDP can readily

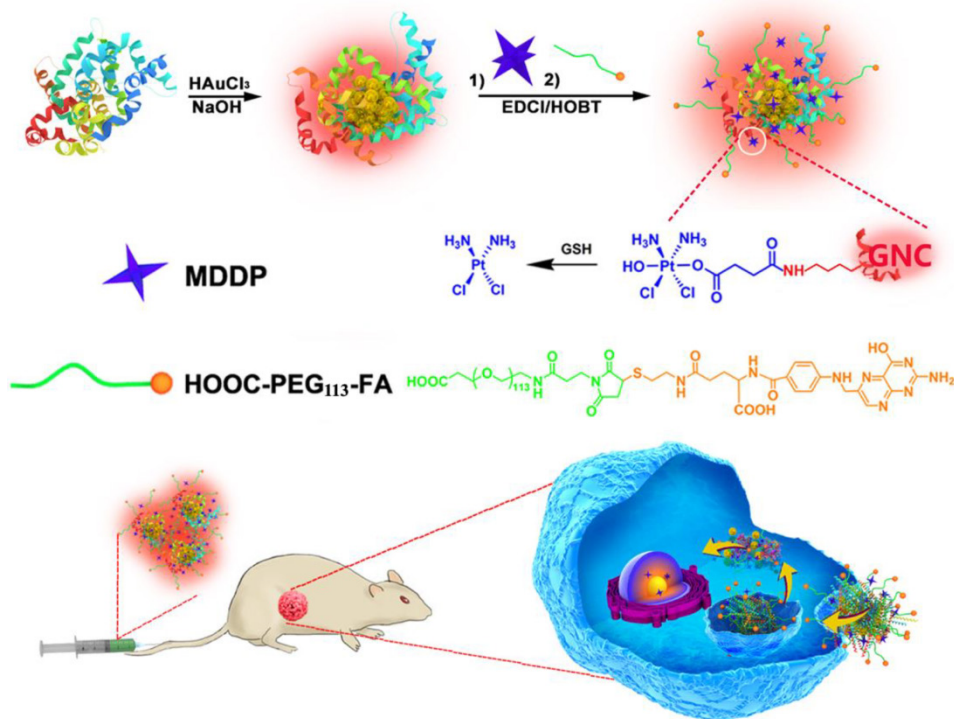


Figure 1. Schematic illustration of GNC-based theranostic nanoplatform for tumor-targeted chemotherapy and fluorescence imaging.

be reduced to cisplatin with glutathione (GSH) as confirmed by high performance liquid chromatography/mass spectrometry (HPLC/MS) measurement (Fig. S4). This is in good consistence with the literature report.(27) The resulting GNC-MDDP nanoparticles were then functionalized with FA-PEG5k-COOH to obtain FA-GNC-Pt for tumor targeted fluorescence imaging and drug delivery. To conjugate FA on GNC nanoparticles, FA molecular was firstly coupled with 2-aminoethyl disulfide pyridine and then reduced with Tris(2-carboxyethyl) phosphine (TCEP) to obtain 2-aminoethylthiol FA (Fig. S5).

It has been well defined that modification of the γ carboxylate group of FA insignificantly impairs the binding affinity of FA with the FR- α .(28) To verify the successful conjugation of 2-aminoethyl disulfide pyridine on the γ carboxylate group of FA, We used to $^1\text{H-NMR}$ spectrum to examine the chemical structure of 2-aminoethyl disulfide pyridine FA. The triplicate peak assigned to the proton of the methylene group next to the γ -carboxylate group split into a broad peak after coupled 2-aminoethyl disulfide pyridine with FA. In contrast, the chemical shift and peak shape of the proton assigned to α -methylene group was not changed (Fig. S6), implying the formation of the amide bond between the γ -carboxylate group of FA and the amine group of 2-aminoethyl disulfide pyridine. 2-aminoethylthiol FA was conjugated on MAL-PEG5k-COOH through the Michael addition between the thiol group and the double bond of the maleimid group (Fig. S7 for $^1\text{H-NMR}$ spectra of FA-PEG5k-COOH).

FA-functionalized PEG spacer was then conjugated on the GNC-Pt nanoparticles via the amidation reaction between the carboxylate group of PEG and the ϵ -amine groups of the lysine residue in BSA (Fig. 1). The synthesis of FA-GNC-Pt nanoparticles was successively examined by UV-Vis spectroscopic examination. The absorption of GNC-Pt nanoparticles increased at 365 nm after grafted with FA-PEG5k-COOH, confirming the successful conjugation of FA on GNC nanoparticles. Five FA molecules were found on each GNC nanoparticle as determined using UV-Vis spectrophotometric measurement (Fig. S8). To do that, we firstly established a standard curve by measuring the absorption of FA-PEG-COOH at 365 nm, and then calculated the FA grafting density by measuring the absorption increase at 365 nm of GNC-Pt suspension before and after FA-PEG conjugation, respectively.

GNC nanoparticles displayed negligible UV-Vis absorption at 540 nm after modified with the MDDP prodrug and FA-PEG spacer, implying no GNC aggregate formed during the conjugation reaction. MDDP modification impaired around 30% fluorescence emission of GNC nanoparticles due to the heavy atom effect of Pt compounds for fluorescence quenching.(29) Conjugation of FA-PEG showed negligible influence on the fluorescence emission of the GNC-Pt nanoparticles (Fig. 2a). In order to elucidate the rule of FA-conjugation on the cellular targeting effect of the GNC nanoparticles, a FA-free PEG spacer was conjugated on MDDP-modified GNC to obtain GNC-Pt nanoparticles.

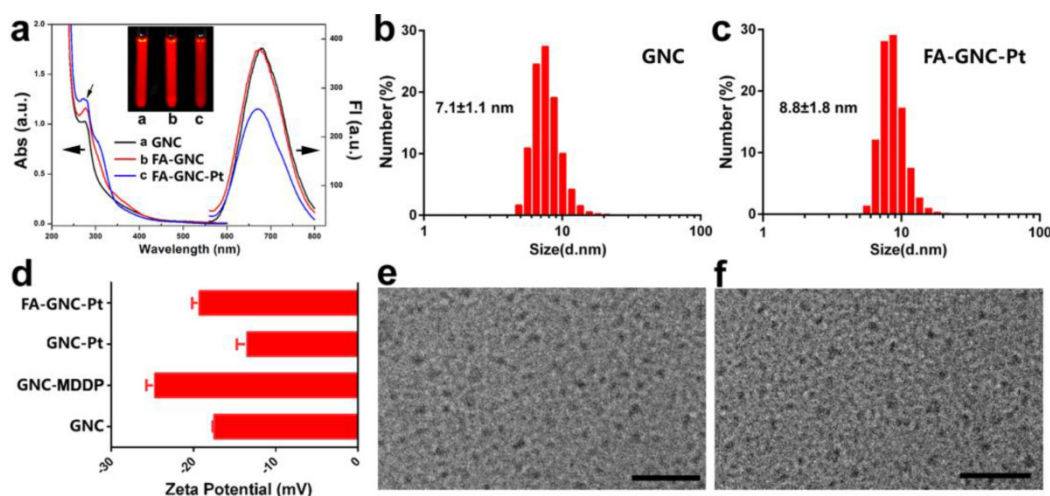


Figure 2. Characterization of FA and cisplatin-conjugated GNC nanoparticles. (a). UV-Vis and fluorescence spectrum of the GNC, FA-GNC and FA-GNC-Pt nanoparticles. Insert showed the fluorescence image of GNC, FA-GNC and FA-GNC-Pt aqueous solution; (b&c) Dynamic light scattering (DLS) determined particle size distribution of (b) parental GNC and (c) FA-GNC-Pt composite nanoparticles; (d) Surface charge of GNC, GNC-MDDP, GNC-Pt and FA-GNC-Pt nanoparticles; (e&f) TEM images of (e) the parental GNC, and (f) the FA-GNC-Pt nanoparticles (scale bar 50 nm).

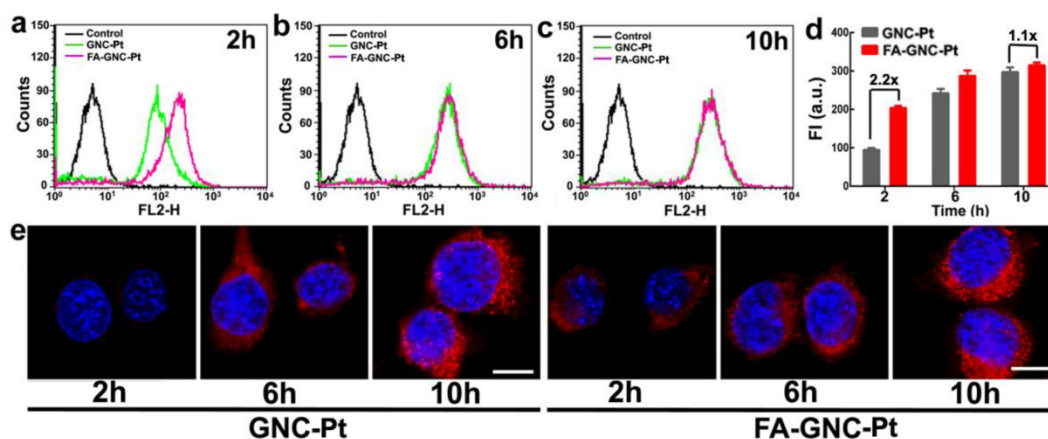


Figure 3. Incubation-time dependent intracellular uptake and distribution of the FA-GNC-Pt nanoparticles. (a-c) Flow cytometric curves of FA-GNC-incubated 4T1 examined after (a) 2, (b) 6 or (c) 10 h incubation; (d) Intracellular fluorescence intensity of 4T1 cells incubated with the GNC-Pt or FA-GNC-Pt nanoparticles; (e) CLSM images of 4T1 cells incubated with the GNC-Pt or FA-GNC-Pt nanoparticles (scale bar 50 μ m).

The particle size of GNC and FA-GNC-Pt nanoparticles was determined using dynamic light scattering (DLS) examination. **Fig. 2b&c** showed that the hydrodynamic diameter of GNC nanoparticles increased by 24% from 7.1 ± 1.1 nm to 8.8 ± 1.8 nm after conjugated with three MDDP and five FA-PEG molecules. The influence of MDDP conjugation on the surface charge was examined using zeta potential measurement. The surface charge of GNC decreased from -18.0 mV to -25.0 mV when conjugated with MDDP since the amino groups of the lysine residues were consumed during the coupling reaction. After FA-PEG conjugation, the surface charge of the resulting FA-GNC-Pt increased slightly to -21.0 mV due to the shielding effect of the PEG corona (**Fig. 2d**). Conjugation of MDDP and FA-PEG did not induce aggregation of GNC nanoparticles as confirmed by transmission electron microscopic (TEM) measurement (**Fig. 2e&f**). ICP-MS measurement revealed that over 65% of cisplatin conjugated on GNC-Pt nanoparticles was released in 8 h in the presence of 5.0 mM GSH (**Fig. S9**) mimicking the intracellular reduction condition of the cancer cells.(30) In contrast, less than 20% of cisplatin was liberated from GNC-Pt nanoparticles in the absence of GSH. The cisplatin release profile implied that cisplatin can efficiently be released from the GNC-Pt nanoparticles via GSH reduction.

Intracellular uptake and distribution of FA-GNC-Pt nanoparticles

We next examined the tumor targeting ability of FA-GNC-Pt nanoparticles using flow cytometric measurement. As shown in **Fig. 3a-d**, FA modification significantly increased the fluorescence intensity after 2 h incubation with the GNC nanoparticles. For instance, 2-fold higher fluorescence intensity was found in FA-GNC-Pt treated 4T1 cells than that detected in

the cells incubated with GNC-Pt. The fluorescence intensity of FA-GNC-Pt treated cells became comparable with that of the cells incubated with PEG-GNC-Pt over time (*e.g.*, 10 h). The increased cellular uptake of FA-GNC-Pt nanoparticles was confirmed by confocal laser scanning microscopic (CLSM) examination. 4T1 cells treated with FA-GNC-Pt nanoparticles exhibited much stronger fluorescence intensity than that in the cells treated with GNC-Pt nanoparticles 2 h post nanoparticle incubation. The fluorescence spots mainly located surrounding the cellular nuclei, indicating the GNC-Pt nanoparticles were entrapped inside the lysosome vesicles.(31) The flow cytometric and CLSM data consistently confirmed that FA modification significantly accelerated the internalization of the FA-GNC-Pt nanoparticles due to the specific interaction between FA and the folate receptor.(32) The cellular uptake of the FA-GNC-Pt nanoparticles can be blocked by pretreating the 4T1 cells with free folic acid, further confirming the accelerated internalization of the FA-GNC-Pt nanoparticles was caused by the specific interaction between folic acid and FR- α (**Fig. S10**). Notably, the intracellular fluorescence intensity determined by flow cytometric measurement became comparable at 6 or 10 h post nanoparticle incubation (**Fig. 3e**). A similar phenomenon was also observed in our previous investigation,(33) and the literature report.(34) This might imply that FA modification insignificantly increased the total amount of the nanoparticles entering the cells although it strongly accelerates the internalization of the nanoparticles.

Cytotoxicity of FA-GNC-Pt nanoparticles *in vitro*

The cytotoxicity of FA-GNC-Pt nanoparticles was evaluated in 4T1 cells by using MTT assay. We

firstly treated 4T1 cells with various formulations for 4 or 36 h, and then measured the cell viability at 36 h post nanoparticle addition. As shown in **Fig. 4a**, after 4 h incubation, FA-GNC-Pt nanoparticles displayed the much higher cytotoxicity than CDDP, GNC-Pt or MDDP. The cytotoxicity of FA-GNC-Pt and GNC-Pt nanoparticles became comparable while notably increased when the incubation time was elongated to 36 h (**Fig. 4b**). To quantitatively compare the cytotoxicity of FA-GNC-Pt and GNC-Pt nanoparticles, their IC₅₀ values post 36 h incubation were calculated and included in **Fig. 4c**. GNC-Pt nanoparticles displayed an IC₅₀ value of 23.1 μM, 4.4-fold lower than that of the MDDP prodrug. The IC₅₀ value of GNC-Pt nanoparticles was further reduced to 17.5 μM by modifying with FA, which was 5.8 and 1.8-fold lower than that of the MDDP prodrug and the GNC-Pt nanoparticles, respectively. It has been reported by Wooly *et al* that the cytotoxicity of cisplatin was notably suppressed by complexed it on the shell of a shell-crosslinked micelle nanoparticles.(35) This might be caused by the limited release of cisplatin payload from the nanoparticles (less than 30% of cisplatin payload was released in 120 h). In contrast, over 65% of MDDP con-

jugated on the GNC nanoparticles was efficiently converted to cisplatin and released from the nanoparticles in 6 h in the presence of 5.0 mM GSH. Moreover, the internalization of MDDP might also be improved by conjugating on GNC nanoparticles since MDDP is highly water soluble and hard to trans-cross the cell membrane.(27) These two factors might synergistically contribute to the improved cytotoxicity of the MDDP prodrug.

We further compared the cytotoxicity of GNC-Pt and FA-GNC-Pt nanoparticles by apoptosis analysis. As shown in **Fig. 4d-g**, after 4h incubation, FA-GNC-Pt nanoparticles induced 16% of 4T1 cells to be in early or late stage of apoptosis, 1.8-fold more efficient than GNC-Pt nanoparticles. The apoptosis percentage of 4T1 cells treated with FA-GNC-Pt increased notably when the incubation time was increased to 36 h as that found by MTT assay (**Fig. 4h-k**). The MTT assay and apoptosis analysis data suggested that FA-GNC-Pt nanoparticles efficiently delivered MDDP prodrug into 4T1 cells via FA-enhanced internalization, where MDDP was reactivated by GSH-mediated reduction or other mechanisms.

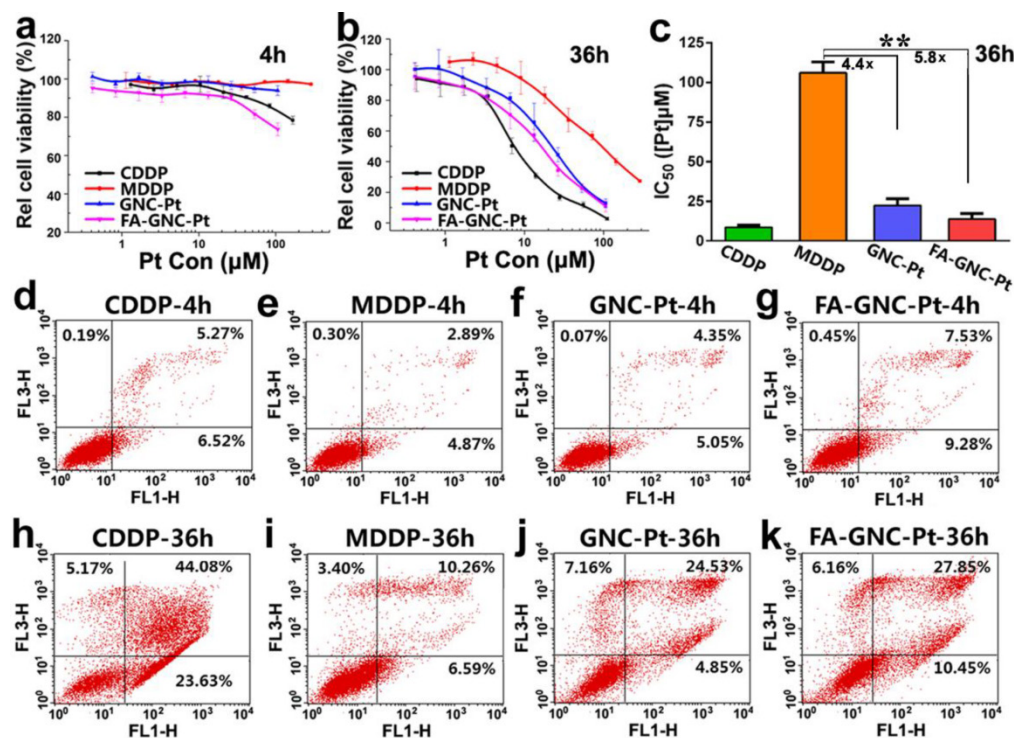


Figure 4. Cytotoxicity assay of the FA-GNC-Pt nanoparticles in 4T1 cells. (a-b) MTT assay determined relatively cell viability of 4T1 cells after treated with the FA-GNC-Pt nanoparticles for (a) 4 or (b) 36 h; (c) MTT assay determined IC₅₀ value of CDDP, MDDP, GNC-Pt and FA-GNC-Pt post 36 h incubation (** p < 0.01); (d-k) Cellular apoptosis induced with CDDP, MDDP, GNC-Pt or FA-GNC-Pt examined post (d-g) 4 h or (h-k) 36 h incubation.

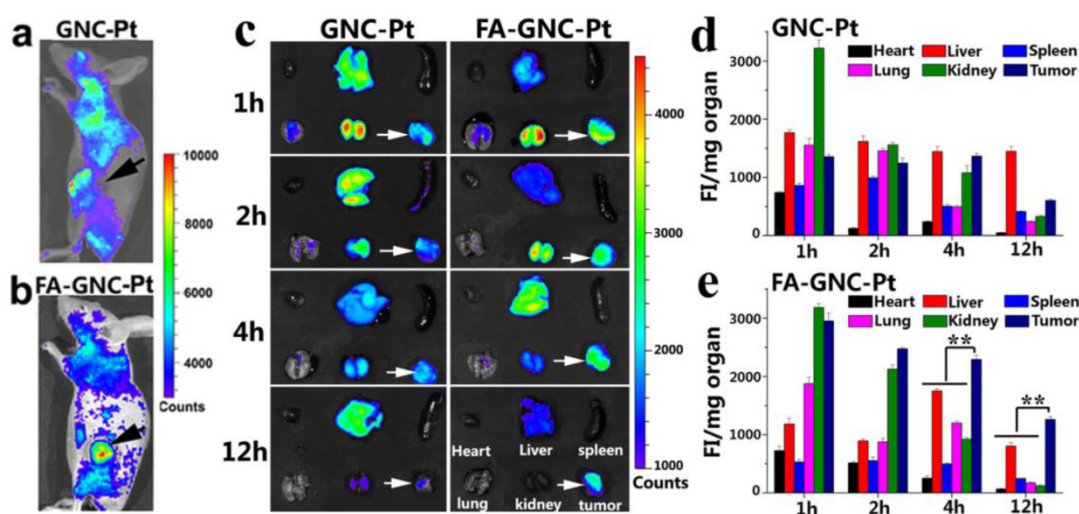


Figure 5. *In vivo* and *ex-vivo* fluorescence imaging and organ distribution of the FA-GNC-Pt or GNC-Pt nanoparticles in 4T1 tumor-bearing nude mice. (a&b) Representative fluorescence images for *in vivo* distribution of (a) GNC-Pt and (b) FA-GNC-Pt nanoparticles examined 2 h post i.v. injection; (c) *Ex-vivo* distribution of the GNC-Pt and FA-GNC-Pt nanoparticles examined at different time points post injection (the white arrows showed the location of tumor, the organs layout was shown in right bottom and applied for *ex-vivo* images); (d&e) Semi-quantitative analysis of (d) GNC-Pt or (e) FA-GNC-Pt distribution in the major organs as determined by normalizing the fluorescence intensity with the organ mass (** $p < 0.01$).

Biodistribution of FA-GNC-Pt nanoparticles *in vivo*

We next performed fluorescence imaging to evaluate the *in vivo* distribution of FA-GNC-Pt nanoparticles. The whole animal fluorescence images clearly demonstrated tumor targeted distribution of FA-GNC-Pt nanoparticles 2 h post tail vein injection (Fig. 5a&b). The major organs (*i.e.*, heart, liver, spleen, lung and kidney) and the tumors were collected at the desired time points post nanoparticle administration. The organ fluorescence intensity was integrated, reduced with the background noise and normalized with the organ mass. As shown in Fig. 5c-e, GNC-Pt nanoparticles reached the highest tumor distribution 2 h post injection, and decreased quickly over time, implying the GNC-Pt nanoparticles were eliminated through the blood circulation. On the contrary, FA-GNC-Pt nanoparticles displayed the highest tumoural accumulation 1 h post nanoparticle injection and then decreased slowly. Moreover, FA-GNC-Pt displayed higher tumoural fluorescence intensity than GNC-Pt at all the time points examined. For instance, the tumoral fluorescence intensity of FA-GNC-Pt group was 2.3-fold higher than that of GNC-Pt one. The difference was amplified by 5.5-fold when examined at 12 h post nanoparticle administration, implying the tumoural distribution and retention of GNC-Pt nanoparticles was significantly enhanced by modified with FA ligand.

Both GNC-Pt and FA-GNC-Pt nanoparticles predominantly distributed in the kidney and tumor in comparison with the spleen, liver, heart, and lung at the early stage post nanoparticle injection (*i.e.*, 1 and 2 h), implying both of them could escape the RES ab-

sorption (Fig. 5c-e). The kidney concentration of GNC-Pt and FA-GNC-Pt nanoparticles decreased stepwise due to renal clearance. Notably, although FA-GNC-Pt nanoparticles displayed increased liver accumulation at the first 4 h post injection, they were cleared rapidly due to their small hydrodynamic particle size.(21) The organ biodistribution data clearly suggested that FA-modified GNC-Pt fluorescence nanoparticles could efficiently escape from the RES capture and realize kidney clearance.

Anti-tumor and biosafety assay of FA-GNC-Pt nanoparticles

The anti-tumor property of FA-GNC-Pt nanoparticles was evaluated in 4T1 tumor bearing nude mouse model. To do that, 4T1-Luc breast cancer cells were subcutaneously injected on the right mammary gland of the nude mice. The mice were randomly grouped when the tumor volume reached 100 mm³, and then i.v. injected with CDDP, MDDP, GNC-Pt or FA-GNC-Pt at an identical Pt dose of 1 mg/kg. The nude mice injected with PBS or GNC nanoparticles were set as negative control. GNC-Pt nanoparticles displayed good anti-tumor ability to delay 65% of tumor growth in compared with that of the PBS group (Fig. 6a). This implied that although the fluorescence imaging data showed that the majority of the GNC-Pt nanoparticles were cleared off in 12 h post i.v. injection through blood flow (Fig. 5c), the MDDP prodrug retained in the tumor and internalized by the cancer cells was still sufficient to suppress proliferation of the cancer cells. FA-GNC-Pt nanoparticles showed significantly better anti-tumor property to inhibit over 80% of the tumor growth, which could be attributed to the synergetic effect between the EPR effect and

FA-enhanced tumoral accumulation and cellular uptake of FA-GNC-Pt. GNC nanoparticles showed negligible influence on the tumor growth, further confirming that the anti-tumor effect of the GNC-Pt and FA-GNC-Pt nanoparticles was attributed to the cytotoxicity of cisplatin, reduced from MDDP.

The 4T1 tumor model selected in this study is also highly aggressive for lung metastasis. Therefore, we examined the lung metastasis suppression efficiency of FA-GNC-Pt nanoparticles at the end of anti-tumor studies. The lungs were freshly collected, photographed, examined by bioluminescence imaging (BLI) and hematoxylin-eosin (H&E) staining, respectively. The photographs of the lungs clearly showed the formation of metastatic lesions in the lungs of MDDP and CDDP groups, comparable to that in PBS and GNC groups (Fig. 6b). In contrast, the lung metastasis of 4T1 cells was significantly inhibited with the FA-GNC-Pt nanoparticles. Moreover, 6.5 ± 0.5 metastasis lesions were found in each lung of the FA-GNC-Pt mouse group, 53.8% less than that found

in the GNC-Pt group, confirming statistically better anti-metastasis ability of FA-GNC-Pt nanoparticles than GNC-Pt. The superior anti-metastasis property of FA-GNC-Pt was further confirmed by BLI examination, metastasis lesion counting and H&E staining, respectively (Fig. 6c&d). This can be most likely explained by the good ability of the FA-GNC-Pt nanoparticles to inhibit the growth of the primary tumor, and successively suppress the metastasis potential of the cancer cells.(36)

The systemic toxicity of the FA-GNC-Pt nanoparticles was evaluated by H&E staining of the major organs (*i.e.* liver, spleen and kidney). As shown in Fig. 7, although CDDP caused obvious tubular atrophy and necrosis due to its severe nephrotoxicity, FA-GNC-Pt nanoparticles did not induce notable histological change of the kidney, as well as the liver and spleen. FA-GNC-Pt nanoparticles caused unobvious body weight change (Fig. S11). The H&E and body weight data consistently confirmed a good biocompatibility of the FA-GNC-Pt nanoparticles.

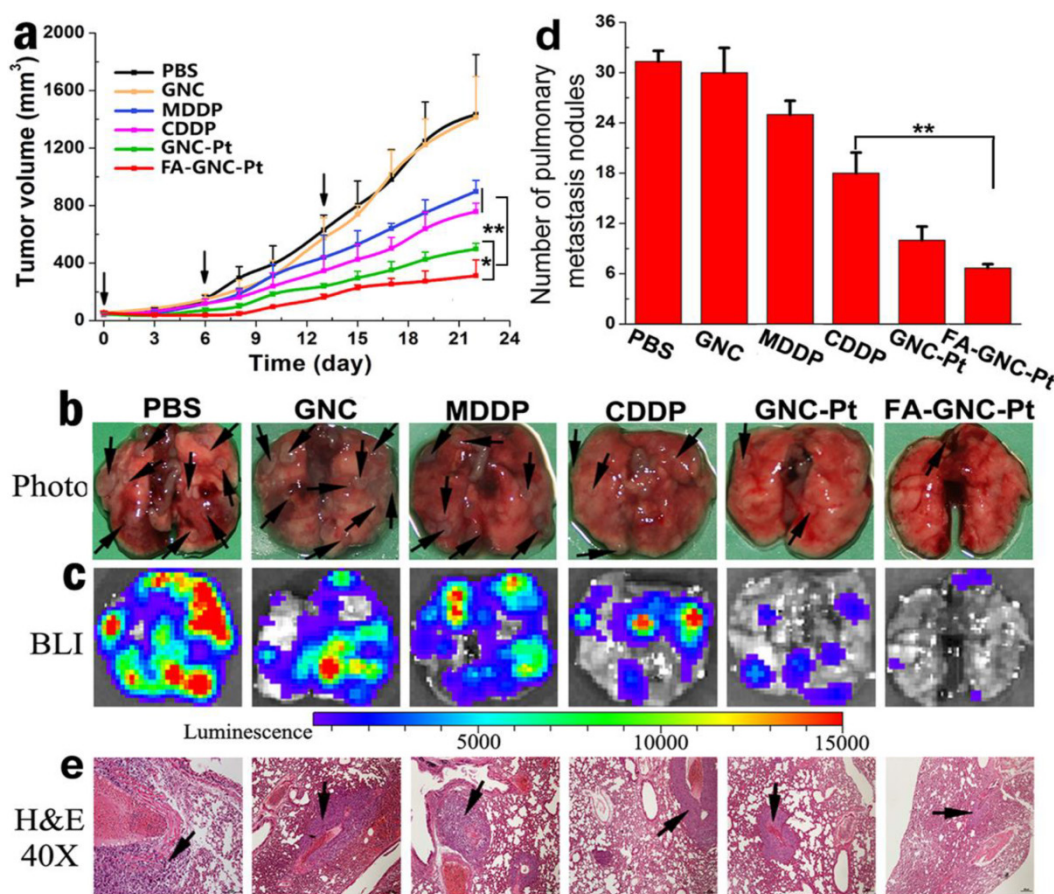


Figure 6. Anti-tumor activity of the FA-GNC-Pt nanoparticles in 4T1 tumor bearing nude mice. (a) Tumor growth curves of different treatment in a mouse model bearing 4T1 tumors after treatment with various formulations (* $p < 0.05$; ** $p < 0.01$); Lung metastasis of 4T1 breast tumor examined by (b) Photo, (c) Bioluminescence imaging, (d) metastasis nodule counting, and (e) H&E staining, respectively (the black arrows indicated the location of metastasis nodules in the lung).

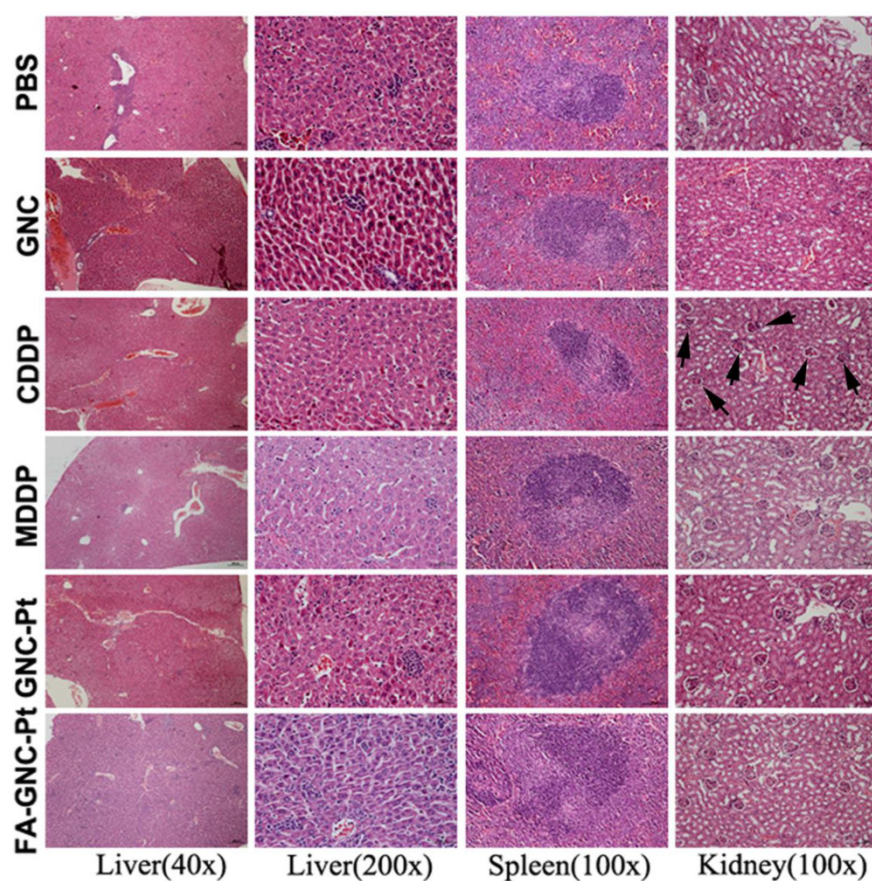


Figure 7. Histopathological examination of the major organs (i.e., liver, spleen and kidney) at the end of the animal studies. The black arrows in the CDDP group indicated tubular atrophy and necrosis.

A pioneer study reported by Lippard *et al.* exploited targeted delivery of MDDP prodrug by using FA-modified single walled carbon nanotube (SWCN). (28) It was demonstrated that SWCN-based nanoplatform specifically delivered the prodrug to FR- α overexpressed KB cancer cells and the MDDP prodrug could be reactivated to crosslink nuclear DNA inside the cells. Although promising, the anti-cancer study was conducted in cell culture level only. The biosafety issue might be another concern for medical application of SWCN-based drug delivery system. In contrast, we employed BSA-protected GNC nanoparticle as a dual-functional nanoplatform in this study for targeted delivery of the cisplatin prodrug and fluorescent tumor imaging, which is of several advantages over that based on SWCN. Firstly, GNC nanoparticles are biodegradable and biocompatible since we used BSA serum protein for nanoparticle synthesis. For clinical translation, BSA can be replaced with human serum protein (HSA) without obviously changing the chemo-physical properties of the nanoparticles (data not shown). Secondly, the prodrug and FA dual-conjugated GNC nanoparticles could selectively accumulate in orthotopic 4T1 tumor model. The nanoparticles displayed high fluorescence

signal for nanoparticle tracking and tumor imaging. The nanoparticles could efficiently inhibit the growth of the primary tumor and suppress the metastasis of the cancer cells to the lung. Moreover, the hydrodynamic diameter of FA-GNC-Pt is in several to ten nanometers, thus allows escape from RES absorption in the liver and quick kidney clearance, which can avoid liver accumulation and minimize the side effect of FA-GNC-Pt nanoparticles.

Conclusion

In summary, we reported a GNC-based theranostic nanoplatform for targeted fluorescence imaging and chemotherapy of the metastatic breast cancer. The GNC nanoparticles were covalently conjugated with a targeting ligand of FA and a cisplatin prodrug MDDP. The nanoparticles induced significant cellular apoptosis upon intracellular activation of the cisplatin prodrug. An *in vivo* distribution assay showed that the FA-GNC-Pt nanoparticles efficiently escaped the RES capture and actively accumulated in the orthotopically implanted breast tumor. The nanoparticles also displayed high efficiency to simultaneously inhibit the growth and lung metastasis of 4T1 breast tumor. All these results suggested a good po-

tential of the FA-modified GNC nanoparticles for cancer theranostic.

Supplementary Material

Supplementary figures, supplementary methods, characterization of the cisplatin prodrug and folic acid conjugated PEG spacer.

<http://www.thno.org/v06p0679s1.pdf>

Acknowledgements

The authors thank Prof. X.Y. Gao from the Institute of High Energy Physics, Chinese Academy of Sciences for advice for GNC synthesis. Financial support from the National Basic Research Program of China (2013CB932704), the National Natural Science Foundation of China (81373359 and 81521005) and the Youth Innovation Promotion Association CAS is gratefully acknowledged.

Competing Interests

The authors have declared that no competing interest exists.

References

- Ma X, Zhao Y, Liang X. Theranostic nanoparticles engineered for clinic and pharmaceuticals. *Acc Chem Res*. 2011;44:1114-22.
- Kumar R, Shin W, Sunwoo K, Kim W, Koo S, Bhuniya S, Kim J. Small conjugate-based theranostic agents: an encouraging approach for cancer therapy. *Chem Soc Rev*. 2015;44:6670-83.
- Huang X, El-Sayed I, Qian W, El-Sayed M. Cancer cell imaging and photothermal therapy in the near-infrared region by using gold nanorods. *J Am Chem Soc*. 2006;128:2115-20.
- Zhang Z, Wang J, Chen C. Gold nanorods based platforms for light-mediated theranostics. *Theranostics*. 2013;3:223-38.
- Gao X, Cui Y, Levenson R, Chung L, Nie S. *In vivo* cancer targeting and imaging with semiconductor quantum dots. *Nat Biotechnol*. 2004;22:969-76.
- Li X, Li H, Liu G, Deng Z, Wu S, Li P, Xu Z, Xu H, Chu P. Magnetite-loaded fluorine-containing polymeric micelles for magnetic resonance imaging and drug delivery. *Biomaterials*. 2012;33:3013-24.
- Nasongkla N, Bey E, Ren J, Ai H, Khemtong C, Guthi J, Chin S, Sherry A, Boothman A, Gao J. Multifunctional polymeric micelles as cancer-targeted, MRI-ultrasensitive drug delivery systems. *Nano Lett*. 2006;6:2427-30.
- Zhang Z, Wang L, Wang J, Jiang X, Li X, Hu Z, Ji Y, Wu X, Chen C. Mesoporous silica-coated gold nanorods as a light-mediated multifunctional theranostic platform for cancer treatment. *Adv Mater*. 2012;24:1418-23.
- Lartigue L, Hugouenq P, Alloeyau D, Clarke S, Levy M, Bacri J, Bazzi R, Brougham D, Wilhelm C, Gazeau F. Cooperative organization in iron oxide multi-core nanoparticles potentiates their efficiency as heating mediators and MRI contrast agents. *ACS Nano*. 2012;6:10935-49.
- Cabral H, Kataoka K. Progress of drug-loaded polymeric micelles into clinical studies. *J Control Release*. 2014;190:465-76.
- Barenholz Y. Doxil(R)—the first FDA-approved nano-drug: lessons learned. *J Control Release*. 2012;160:117-34.
- Boulikas T. Clinical overview on Lipoplatin: a successful liposomal formulation of cisplatin. *Expert Opin Inv Drug*. 2009;18:1197-218.
- Dranitsaris G, Yu B, Wang L, Sun W, Zhou Y, King J, Kaura S, Zhang S, Yuan P. Abraxane(R) versus Taxol(R) for patients with advanced breast cancer: A prospective time and motion analysis from a Chinese health care perspective. *J Oncol Pharm*. 2014;17:A737
- Yu H, Cui Z, Yu P, Guo C, Feng B, Jiang T, Wang S, Yin Q, Zhong D, Yang X, Zhang Z, Li Y. pH- and NIR light-responsive micelles with hyperthermia-triggered tumor penetration and cytoplasm drug release to reverse doxorubicin resistance in breast cancer. *Adv Funct Mater*. 2015;25:2489-500.
- Park K. Controlled drug delivery systems: past forward and future back. *J Control Release*. 2014;190:3-8.
- Chen Q, Liang C, Wang C, Liu Z. An imagable and photothermal "Abraxane-like" nanodrug for combination cancer therapy to treat subcutaneous and metastatic breast tumors. *Adv Mater*. 2015;27:903-10.
- Chen L, Wang C, Yuan Z, Chang H. Fluorescent gold nanoclusters: recent advances in sensing and imaging. *Anal Chem*. 2015;87:216-29.
- Zhang CL, Li C, Liu Y, Zhang J, Bao C, Liang S, Wang Q, Yang Y, Fu H, Wang K, Cui D. Gold nanoclusters-based nanoprobe for simultaneous fluorescence imaging and targeted photodynamic therapy with superior penetration and retention behavior in tumors. *Adv Funct Mater*. 2015;25:1314-25.
- Wang Y, Zhou F, Kim P, Xia Y. Protein-protected Au clusters as a new class of nanoscale biosensor for label-free fluorescence detection of proteases. *Small*. 2012;8:3769-73.
- Wang Y, Sun Q, Zhu L, Zhang J, Wang F, Lu L, Yu H, Xu Z, Zhang W. Triplex molecular beacons for sensitive recognition of melamine based on abasic-site-containing DNA and fluorescent silver nanoclusters. *Chem Commun*. 2015;51:7958-61.
- Zhang X, Luo Z, Chen J, Shen X, Song S, Sun Y, Fan S, Fan F, Leong D, Xie J. Ultrasmall Au(10-12)(SG)(10-12) nanomolecules for high tumor specificity and cancer radiotherapy. *Adv Mater*. 2014;26:4565-8.
- Khandelia R, Bhandari S, Pan U, Ghosh S, Chattopadhyay A. Gold nanocluster embedded albumin nanoparticles for two-photon imaging of cancer cells accompanying drug delivery. *Small*. 2015;11:4075-81.
- Wang YL, Cui Y, Zhao Y, Liu R, Sun Z, Li W, Gao X. Bifunctional peptides that precisely biomineralize Au clusters and specifically stain cell nuclei. *Chem Commun*. 2012;48:871-3.
- Zhang X, Luo Z, Chen J, Song S, Yuan X, Shen X, Wang H, Sun Y, Gao K, Zhang L, Fan S, Leong D, Guo M, Xie J. Ultrasmall glutathione-protected gold nanoclusters as next generation radiotherapy sensitizers with high tumor uptake and high renal clearance. *Sci Rep*. 2015;5:8669.
- Zhou C, Long M, Qin Y, Sun X, Zheng J. Luminescent gold nanoparticles with efficient renal clearance. *Angew Chem Int Ed*. 2011;50:3168-72.
- Wang Y, Xu C, Zhai J, Gao F, Liu R, Gao L, Zhao Y, Chai Z, Gao X. Label-free Au cluster used for in vivo 2D and 3D computed tomography of murine kidneys. *Anal Chem*. 2015;87:343-5.
- Xiao H, Qi R, Liu S, Hu X, Duan T, Zheng Y, Huang Y, Jing X. Biodegradable polymer-cisplatin(IV) conjugate as a pro-drug of cisplatin(II). *Biomaterials*. 2011;32:7732-9.
- Dhar S, Liu Z, Thomale J, Dai H, Lippard S. Targeted single walled carbon nanotube mediated Pt(IV) prodrug delivery using folate as homing device. *J Am Chem Soc*. 2008;130:11467-76.
- Varnes A, Dodson R, Wehry E. Interactions of transition-metal ions with photoexcited states of flavins. *Fluorescence quenching studies J Am Chem Soc*. 1972;94:946-50.
- Yu H, Russ V, Wagner E. Influence of the molecular weight of bioreducible oligoethylenimine conjugates on the polyplex transfection properties. *AAPS J*. 2009;11:445-455.
- Wang D, Xu Z, Yu H, Chen X, Feng B, Cui Z, Lin B, Yin Q, Zhang Z, Chen C, Wang J, Zhang W, Li Y. Treatment of metastatic breast cancer by combination of chemotherapy and photothermal ablation using doxorubicin-loaded DNA wrapped gold nanorods. *Biomaterials*. 2014;35:8374-84.
- Feng B, Xu Z, Zhou F, Yu H, Sun Q, Wang D, Yin Q, Zhang Z, Li Y. Near infrared light-actuated gold nanorods with cisplatin-polypeptide wrapping for targeted therapy of triple negative breast cancer. *Nanoscale*. 2015;7:14854-64.
- Yu H, Nie Y, Dohmen C, Li Y, Wagner E. Epidermal growth PAMAM-pentaethylenehexaminefor targeted gene delivery produced by click chemistry. *Biomacromolecules*. 2011;12:2039-47.
- Bruin K. de Ruthardt N, Gersdorff K, von Bausinger R, Wagner E, Ogris M. Cellular dynamics of EGF receptor-targeted synthetic viruses. *Mol Ther*. 2007;15:1297-304.
- Zhang F, Elsbahy M, Zhang S, Lin L, Zou J, Wooley K. Shell crosslinked knedel-like nanoparticles for delivery of cisplatin: effects of crosslinking. *Nanoscale*. 2013;5:3220-5.
- Wang D, Wang T, Xu Z, Yu H, Feng B, Zhang J, Guo C, Yin Q, Zhang Z, Li Y. Cooperative treatment of metastatic breast cancer using host-guest nanoplat-form loading docetaxel and siRNA. *Small*. 2016;12:488-98.